POLITECNICO DI TORINO
Repository ISTITUZIONALE

Design of a Spherical UGV for Space Exploration

Original
Design of a Spherical UGV for Space Exploration / Melchiorre, M., Salamina, L., Mauro, S., Pastorelli, S.. - ELETTRONICO. - (2022). (International Astronautical Congress (IAC) 2022).

Availability:
This version is available at: 11583/2972388 since: 2022-10-18T09:52:20Z

Publisher:
International Astronautical Federation

Published
DOI:

Terms of use:

This article is made available under terms and conditions as specified in the corresponding bibliographic description in the repository

Publisher copyright

(Article begins on next page)

14 November 2026

73rd International Astronautical Congress (IAC), Paris, France, 18-22 September 2022.
Copyright ©2022 by Dr. Matteo Melchiorre. Published by the IAF, with permission and released to the IAF to publish in all forms.

IAC-22,A3,IP,38,x72104

Design of a Spherical UGV for Space Exploration

Matteo Melchiorre*, Laura Salamina, Stefano Mauro and Stefano Pastorelli

Department of Mechanical and Aerospace Engineering, Politecnico di Torino, C.so Duca degli Abruzzi 24, Turin, Italy, matteo.melchiorre@polito.it, laura.salamina@polito.it, stefano.mauro@polito.it , stefano.pastorelli@polito.it
* Corresponding Author

Abstract

The paper presents the design of a spherical UGV (Unmanned Ground Vehicle) for exploration of critical, unknown or extended areas, such as planetary surfaces. Spherical robots are an emerging class of devices whose shape brings many advantages, e.g. omni-directionality, sealed internal environment and protection from overturning. Many dedicated sensors can be safely placed inside the sphere and the robot can roll in any direction without getting stuck in singular configurations. Specifically, the proposed UGV is thought to collect images and environmental data, so required sensors are firstly discussed to evaluate in sequence of the payload in terms of size and energy consumption. The most effective drive mechanism is selected considering several possible concepts and carrying a trade-off process based on the requirements for a space mission. The optimal solution involves the use of a single pendulum: a hanging mass, attached to the central shaft of the sphere, is shifted to produce rolling. The design issues due to the selected mechanism are discussed, showing the effect of design parameters on the expected performance. For instance, the barycenter offset from the center of the sphere plays a crucial role and affects the maximum step or inclines that can be overcomed. Therefore, the pre-design phase is conducted by discussing the functional design of the robot and introducing a differential mechanism for driving and steering. A quasi omni-directionality is achieved and the mechanical components, opportunely designed according to the loads acting on the device, are arranged to match the mission requirements. Moreover, the mechatronic integration is discussed: microcontrollers, drive electronics, sensors and batteries are sized in order to reach 3 hours of continuous operation. The multibody system is finally modelled in Matlab-Simscape to verify the mechanism for the UGV testing in specific cases. Results show that a suitable layout is a 0.5 m diameter spherical UGV with a steel main structure, mounting 2 DC motors that activate a bevel gear by means of pulleys and timing belts. The spherical shell, with the internal mechanism and electronics, has a total mass of 25 kg and from standstill it can climb up to 15 degrees inclines or steps up to 25 mm, as proved by Matlab simulations. Future works will focus on the realization of the physical prototype, as well as navigation and control strategies.

Keywords: spherical robot, UGV, space exploration, robot design, robot modeling

1. Introduction

An UGV is an autonomous robotic system that moves in contact with the ground. Its most common application regards exploration in those cases where human presence is limited or not allowed due to harsh conditions of the environment. An emerging class of UGV is represented by spherical robots. As the name suggests, they are ball-shaped robots and present some advantages over a traditional UGV because of the geometry. They experience less friction due to maintaining only one contact point with the ground. Moreover, due to radial symmetry, spherical robots are free from overturning and potentially omni-directional, i.e. the direction of travel is not affected by the orientation. In addition, the spherical shell can provide a sealed internal environment to host mechanical parts and sensors, and can be designed to challenge uneven terrains as well as to rebound from collisions in a non-destructive manner.

The state of the art of spherical robots can be classified depending on the driving principle [1]. Barycenter offset (BCO) robots generate motion by gravity: the center of mass is shifted so that the ball rolls to a new equilibrium position. The main drawback of this solution is the impossibility to move the center of mass outside the sphere of the robot, thus the maximum driving torque is limited. Different solutions exploit this principle.

A common design of BCO is the hamster ball robot, so called since it resembles a hamster in a toy ball: a wheeled mobile robot is placed inside the sphere and its weight running in the shell determines the motion of the system. A simple prototype is given by [2], where a small four-wheeled vehicle is adopted. However, in [2] the system is not omni-directional, as the rolling direction depends on the orientation of the internal unit. An alternative is described by [3], which use a differential-wheeled robot to achieve omni-directionality. To maintain friction and prevent from overturning of the internal robot, some hamster ball concepts use springs or elements that force the wheels to the inner shell. In this case, the internal unit is referred as IDU (Internal Driving Unit) [4]. For instance, the robot presented in [5] mounts an IDU that achieve also omni-directionality by using a

Copyright ©2022 by Dr. Matteo Melchiorre. Published by the IAF, with permission and released to the IAF to publish in all forms.

mechanism inversed to that in the ball mouse. The most recent works are also featured by omni-directional motion through omni-wheels [6], [7]. From the cited documents, hamster ball systems present several advantages: the design is relatively simple, motion control can be referred to the internal unit and the mass is concentrated near the inner surface of the shell, which allows maximizing the output torque. On the contrary, the inner surface needs to be rigid and as uniform as possible to maintain the friction with the IDU. Moreover, collisions and overturning may cause slippage between wheels and shell, hence the application to irregular terrains is limited.

Another popular solution for BCO robots consists of using a pendulum: a mass hanging from a shaft that passes through the center of the sphere. Shifting the pendulum determines the motion of the sphere in the corresponding direction. Most of the pendulum driven spherical robots in the literature are characterized by a single pendulum, where two perpendicular motors mounted on a gimbal allow forward and lateral swing of the pendulum to drive and steer the sphere [8]–[11]. However, motion is not omni-directional as there is a turning radius related to the orientation of the shaft and the position of the pendulum. A quasi omni-directional solution is the double pendulum presented in [12]: through a synchronous rotation of two pendulums around the pitch axis in opposite direction the sphere can turn in place. Compared to the hamster ball, pendulum robots are not omni-directional, but do not suffer from overturning and can better face collisions. For instance, the shell can be designed with flexible elements as the motion is not resulting from friction between the IDU and the spherical surface. This makes pendulum mechanisms better suited for exploration of irregular grounds. In addition, they have an easy-to-implement design that allows the shell to be sealed.

A different class of BCO robots is represented by unbalanced masses, that consists of a number of masses that translate in a controlled manner along fixed linear guides in order to move the barycenter of the robot. For example, in [13] four masses are displaced using power screwed spokes. A design with three masses guided by mutually perpendicular, non-intersecting axis is presented in [14]. Spherical robots based on unbalanced masses are omni-directional and allow for a more precise barycenter positioning. However, the shell must be rigid, motion control can be challenging and efficiency is limited. In fact, the presence of several masses requires same number of actuators. Moreover, to generate sharp trajectories of the sphere the center of mass must be quickly relocated. This involves high powers actuators, that affect size and weight of the whole robot.

A second family of spherical robot achieve motion by shape transformation (ST), which consists of modifying the shell or reconfigure the shape. The main advantage of being able to transform is a significant enhancement of the cross-obstacles ability, while maintaining some of the spherical shape benefits. On the other hand, mechanics and control architecture have a different design complexity compared to BCO.

An example of ST is the driving shell robot, that uses the interaction between shell elements and the ground to generate forces in the desired direction of motion. It is the case of the concept presented in [15] where the external surface deforms upon electrical stimuli, or the ones in [16], [17] that use individually inflatable cells. The main drawback of this kind of system is the need of actuating and controlling many spherical sectors for a precise trajectory.

Some different models among ST are hybrid robots that use a partial or total reconfiguration to change the propulsion method. For example, the design of an hexapod that can fold the legs to assume a spherical shape is reported in [18]; this allows walking or rolling at will. An hybrid quadruped characterized by similar behaviour is described in [19], where the robot can retract legs inside the spherical shell and roll through a leg kick. The same principle is adopted by the three-legged robot shown in [20] that can reconfigure to a sphere and use legs to push its body forward. An interesting prototype of spherical robot able to roll, crawl, and fly is developed in [21]; these motion modes are obtained by packaging into a sphere a foldable quadcopter and four removable legs. The major strength of hybrid robots is the possibility to alternate a closed configuration to a transformed version that can walk, crawl or fly. This permit to exploit the rolling motion for a less power consumption and to choose the other modalities according to circumstances. In fact, walking or flying abilities improves the capability of obstacle crossing and solves the limited maximum torque problem of pendulum and hamster-ball driven spherical robots. However, hybrid robots represent the most complex class and the large number of mechanical parts makes them less reliable, also limiting the internal volume available for sensors. Moreover, designing a sealed and flexible shell can be problematic as transformation relies on relative motion between spherical sectors.

Finally, it is worth to mention other two emerging families of spherical robots, like drone-actuated (DA) [22], [23] and wind-driven (WD) [24], [25]. In particular, DA robots are made of a drone covered by a spherical shell, so that one can switch between rolling and flying mode. These types of systems show the benefits and limitations of hybrid spherical robots belonging to ST, except for the shell that is not involved in any transformation. As regard WD, they are basically lightweight sensorized spheres carried by the wind. Due to the lack of an active driving system, trajectory cannot be controlled and there is a risk to become wedged.

Copyright ©2022 by Dr. Matteo Melchiorre. Published by the IAF, with permission and released to the IAF to publish in all forms.

This work presents a spherical robot for space exploration that exploit the BCO by a single pendulum. The reasons behind the choice of a pendulum mechanism will be explained by introducing the mission and by carrying out an insightful trade-off to select the motion principle that best fits the requirements. The main contribution with respect to the current state of knowledge is the robot design, which is described step by step by considering sensors, driving mechanism, actuators, control units and mechatronic integration. Some details on the executive design will be also given to discuss material and size of the components, and to point out the feasibility of the proposed solution. At the end, the operation of the robot is simulated in Matlab-Simscape to show simple manoeuvres and to analyze robot performances in different scenarios, like the overcome of steps.

2. Mission specifications

The robot is devised for environmental reconnaissance in critical or uninhabited areas. In Table 1 the characteristics of the system for the design phase are reported.

Table 1. System specifications

Target	Earth, Moon, Mars
Terrain	Clay, Sand, Grass, Mineral, Water
Min. Step height	25 mm
Min. Slope	15°
Min. Velocity	2.5 m/s
Min. Acceleration	0.5 m/s^2
Max. Diameter	0.5 m
Max. Mass	25 kg
Autonomy	3 h
Teleoperated/Autonomous	Autonomous with acquisition system
Omni directionality	✓

The robot must be able to run on different types of terrain, characteristic of Mars, Moon and Earth. Hence, obstacles can be considered as steps or inclinations of the ground. Limits on performances derive from some evaluations about the application of the robot. It is desired that the robot can run at least at human average stroke and that can rapidly change running direction. A fundamental requirement is the possibility to remotely control the robot. In addition, the robot must be equipped with batteries and charging system. In the end, the maximum size of the robot is defined considering the possibility to carry the robot by hand.

A set of commercial off-the-shelf sensors, as well as the data acquisition and transmission system, has been defined for batteries dimensioning. This is needed for preliminary analysis of the first laboratory prototype. An Arduino board is selected for the control of the robot. The components for the prototype have been selected according to the possibility to make some tests on Earth, in order to validate the design solution. For spatial application, the selection of the parts of the robot must be reconsidered.

2.1 Sensors

The sensors are needed to record temperature, pressure and humidity of the environment, radioactivity, gas data, and images.

Climatic data, as temperature pressure and humidity, can be measured using boards of small dimensions. The Adafruit BME-280 has been chosen for this application; it can be easily integrated in the Arduino board and has the characteristics contained in Table 2.

Table 2. Adafruit BME-280 characteristics

Supply voltage	3.3 V
Current consumption	3.6 μA @ 1 Hz
Operation Range, Temperature	$-40 \div 85$ °C
Operation Range, Pressure	$300 \div 1100$ hPa
Operation Range, Humidity	$0 \div 100\%$
Board dimension	$19 \times 18 \times 3$ mm
Mass	1 g

A radioactivity sensor is needed for measuring the quantity of β rays and γ rays. Radioactivity sensors are usually made of a Geiger counter; it consists of a tube filled with an inert gas at low pressure, to which a high voltage is applied. The tube conducts electrical charge when particles of the radiation make the gas conductive because of ionization. This process produces an electric pulse. The quantity of pulses per unit of time defines the radioactivity of the environment. The module chosen for the robot is the Pocket Geiger Radiation Sensor by Sparkfun, having the characteristics in Table 3.

Table 3. Pocket Geiger Radiation Sensor characteristics

Supply voltage	5 V
Current consumption	30 mA
Voltage at Geiger tube	560 V
Acquisition rate	100 Hz
Board dimension	$105 \times 45 \times 25$ mm
Mass	50 g

Gas sensors are necessary to have information about the composition of air. The sensors identified use the principle of the Galvanic cell: according to the percentage of the single gas detected in the air, the output voltage changes. The sensors chosen can identify the presence of oxygen, hydrogen, carbon monoxide and methane, have small dimensions and are quite light.

Copyright ©2022 by Dr. Matteo Melchiorre. Published by the IAF, with permission and released to the IAF to publish in all forms.

The Arducam Mini 2MP Plus – OV2640 SPI Camera Module has been selected for image capturing. The module mounts a 2MP image sensor. It can be easily integrated on the Arduino board in a multicamera configuration, using a specific shield. The characteristics of the camera module are reported in Table 4.

Table 4. Characteristics of Arducam Mini module

Supply voltage	5 V
Current consumption	50 mA
Array size	UXGA 1600 × 1200 @ 15 fps
Board dimension	34 × 24 × 22 mm
Mass	20 g

2.2 Data acquisition and transmission system

A designated Arduino Mega will be in charge of the data acquisition and transmission. An XBee shield has been considered for the wireless communication system, which is based on mesh network and uses a ZigBee protocol. The XBee shield and the Arduino Mega characteristics are in Table 5. The hardware scheme of the acquisition/transmission group is shown in Fig. 1.

Table 5. XBee shield and Arduino Mega characteristics

	Arduino Mega	XBee shield
Supply Voltage	7 – 12 V	3.3 V
Current consumption	50 mA	0 – 215 mA
Board dimension	101 × 53 mm	60 × 53 mm
Mass	37 g	30 g

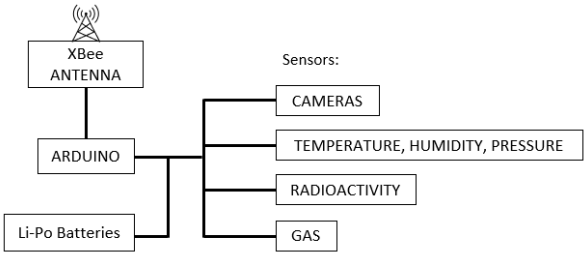

Fig. 1. Hardware scheme of the acquisition/transmission group

2.3 Batteries sizing and volume analysis

The sizing of the batteries necessary to power the sensors chosen allows to have an estimation of their contribution to the bulk and to the weight of the robot. According to what reported in the previous section, sensors need around 500 mA. The battery minimum capacity to allow the sensor group to work for 3 hours is 1590 mAh. A battery having capacity of 1900 mAh is enough for the application. In Table 6 the bulk of the single devices of the system considered are reported.

Table 6. Dimensions of the acquisition/transmission group devices

Device	Weight (g)	Dimensions (mm)	Volume 10^3(mm^3)
Arduino MEGA	37	101 × 53 × 10	53.53
XBee	30	60 × 53 × 10	31.8
BME 280	1	19 × 18 × 3	1.026
Geiger counter	50	105 × 45 × 25	118.1
Gas sensor	24	ϕ28 × 47.3	29.1
Arducam	20 × 4	34 × 24 × 22	18
Battery	105	97 × 36 × 15	52.38

From system specifications, the maximum diameter of the sphere containing the robot is $d = 0.5$ m, so the available volume is:

$$V_s = \frac{4}{3}\pi\left(\frac{d}{2}\right)^3 = 6.545 \cdot 10^{-2}\ \text{m}^3 \quad (1)$$

where V_s is the volume of the sphere. From Table 6, the total volume of the payload is $V_{pl} = 303.936 \cdot 10^{-6}$ m^3, so the percentage of occupied volume is:

$$\frac{V_{pl}}{V_s} = \frac{303.936 \cdot 10^{-6}\text{m}^3}{6.545 \cdot 10^{-2}\ \text{m}^3} = 0.005 \quad (2)$$

This result confirms that the devices are compatible with the maximum size defined by the specifications.

3. Trade off analysis for robot mechanism selection

In order to simplify the choice of the mechanism for the motion of the robot, some parameters have been defined according to Table 1. A weight has been assigned to all the parameters; thus, for each mechanism a score has been given for all parameters by analysing pros and cons outlined by the state of the art.

Some classes of mechanisms have been discarded because of the impossibility to respect some design constraints. WD and DA robots have not been considered because of the lack of controllability and the high complexity, respectively.

Design simplicity indicates the ease of constructing the mechanism. For instance, an hamster ball robot is simpler to build than the other mechanisms. The flexibility of the shell is a fundamental parameter since it determines the capability of the robot to overcome obstacles and adapt to the unevenness of the soil. Power consumption is related to the number and type of actuators, and on the lightness of the robot. Omni-directionality is a desired feature; not all the mechanisms allow omnidirectionality, however most of them can change direction with sharp curvature. The capability to overcome obstacles is meant in the possibility to climb

Copyright ©2022 by Dr. Matteo Melchiorre. Published by the IAF, with permission and released to the IAF to publish in all forms.

an inclined plane or a step. Control simplicity is strictly related to the number of degrees of freedom of the robot. Path accuracy is intended as the possibility to control the sphere on high curvature paths. The innovation of the solution has also been considered.

The parameters and their weights are shown in Table 7. In Table 8 the trade-off is reported. The mechanism with the highest total score has been selected for the design of the robot. The best solution is a spherical robot driven by a single pendulum. It is worth to mention that this class is not omnidirectional, but the results will show that a robot of this type can steer with tight curvature radius, achieving a quasi omni-directionality.

Table 7. Trade-off parameters and weight

Parameter	Weight
Omnidirectionality	5
Path accuracy	5
Get past obstacles ability	4
Innovation	4
Power consumption	4
Shell flexibility	4
Lightness	3
Design simplicity	2
Control simplicity	1

4. Study of the driving mechanism

In this section the single pendulum is primarily studied from functional point of view to highlight some important relationships between geometry and performance. After, a design solution that takes full advantage of BCO is shown.

4.1 Functional analysis

The maximum driving torque of BCO robots is limited by the offset of the center of mass, that is contained within the sphere radius. For this, it is important to discuss how geometry and inertia affect robot capabilities, with a view on mission specifications.

4.1.1 Analysis of step and incline

Let G denote the center of mass of the system. Let a denote the distance between the center of the sphere and G. By observing the limit cases in Fig. 2, the maximum incline angle φ and step height h are given by the followings:

$$\varphi = \sin^{-1}\frac{a}{r} \tag{3}$$

$$h = r - \sqrt{r^2 - a^2} \tag{4}$$

where r is the sphere radius. Equations (3) and (4) are represented by the curves in Fig. 3. It is clear that r and a play an important role in the design phase.

In general, there is a compromise between the offset a and the maximum driving torque. In fact, the higher a, the higher the driving torque, the larger the size of the actuator, that in turn affect the offset.

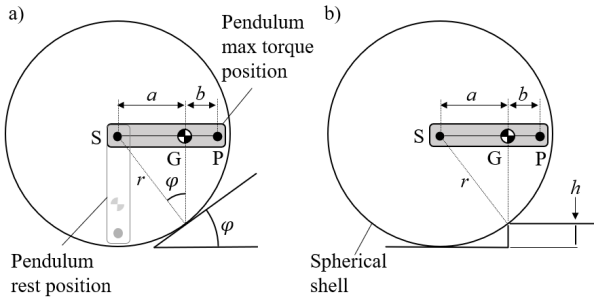

Fig. 2. Analysis of limit cases of incline (a) and step (b)

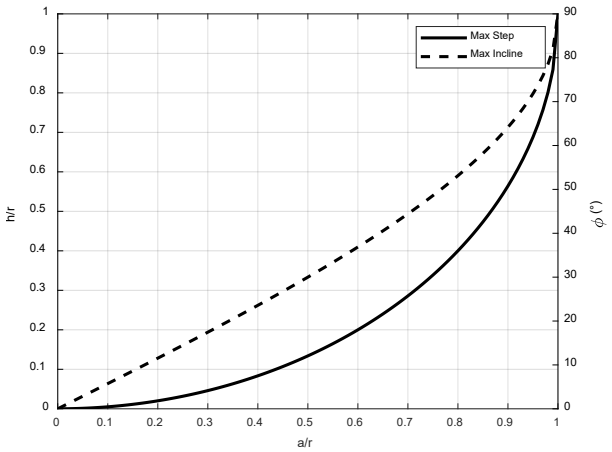

Fig. 3. Relationships between the barycentre offset, the sphere size and the maximum step or incline

As in practice designing a system with high value of a/r is challenging, it is reasonable to choose the maximum size for the sphere. In fact, a large radius helps to generate greater torque and resistive torque from environmental objects such as stones or doorsteps remains low [26]. In the present case, by considering the maximum radius and the minimum step height, from (4) one can find the minimum value of the ratio a/r that satisfies the requirements:

$$\frac{h_{min}}{r_{max}} = 0.1 \quad \Rightarrow \quad \left(\frac{a}{r}\right)_{min} \simeq 0.44 \tag{5}$$

In fact, in correspondence of $a/r = 0.44$ it is $\varphi \simeq 26°$, thus the required minimum incline angle is also largely verified.

Copyright ©2022 by Dr. Matteo Melchiorre. Published by the IAF, with permission and released to the IAF to publish in all forms.

Table 8. Trade-off scores

			SPHERICAL ROLLING ROBOT								
			Gravity							Shape transformation	
			Hamster ball robot				Pendulum driven		Unbalanced Mass	Shell driven	Hybrid
			4-wheeled	Differential	Single	Ball	Single	Double			
		WEIGHT									
DESIGN	Simplicity	**2**	5	5	4	3	4	2	2	1	1
	Shell flexibility	**4**	1	1	2	2	5	5	1	2	2
PERFORMANCE	Power economy	**4**	4	4	4	4	3	2	1	3	4
	Lightness	**3**	5	5	4	4	3	1	1	2	3
	Omnidirectional	**5**	2	4	4	5	2	4	4	4	4
	Obstacles	**4**	2	2	2	2	2	2	2	4	4
CONTROL	Simplicity	**1**	5	4	4	4	4	2	1	1	1
	Path accuracy	**5**	2	2	3	3	5	5	5	1	2
	Innovation	**4**	1	1	1	2	3	4	4	5	5
			82	**91**	**95**	**102**	**108**	**106**	**85**	**90**	**102**

In the design phase, paying attention to the mass of the shell m_s and the one of the pendulum m_p is important to realize the minimum value a/r. For instance, let b indicate the distance between the center of mass of the pendulum P and the one of the whole system G. Let S denote the center of mass of the spherical shell. By observing Fig. 2, the following equation holds:

$$a(m_s + m_p) = m_p(a + b) \tag{6}$$

and dividing by r, (6) becomes:

$$\frac{a}{r} = \frac{m_p}{m_s}\frac{b}{r} \tag{7}$$

By substituting (5) in (7) one can find the relationship between the representative inertial and geometric properties of the system that satisfy the minimum requirements on step and incline.

4.1.2 Analysis of the acceleration

Consider a pendulum-driven spherical robot rolling on a plane in pure rolling condition as shown in Fig. 4. Assume that the unbalance is maintained during the forward motion of the sphere thanks to an actuator placed at the joint S, that provides an internal torque between the spherical shell and the pendulum. As a first approximation, the oscillation of the pendulum near the equilibrium angle θ_p is neglected. By indicating with $\ddot{p}_s$ the x-axis component of the acceleration of the sphere and with $\ddot{\theta}_s$ the angular acceleration, the system dynamics is described by:

$$\begin{cases} m\ddot{p}_s - F = 0 \\ N - mg = 0 \\ I_s\ddot{\theta}_s + mga\sin\theta_p - rF = 0 \end{cases} \tag{8}$$

where $m = m_s + m_p$ is the total mass of the robot, F is the friction force, N is the normal force, g is the gravitational acceleration and I_s is the moment of inertia of the spherical shell. Because of the pure rolling constraint, it is $\ddot{p}_s + r\ddot{\theta}_s = 0$. Thus, third equation of (8) gives:

$$\ddot{p}_s = \frac{r(m_s + m_p)ga\sin\theta_p}{I_s + (m_s + m_p)r^2} \tag{9}$$

In the maximum torque configuration it is $\theta_p = 90°$ (see Fig. 2). By recognizing (6) in the numerator of (9), one can write:

$$\ddot{p}_s = \frac{rm_p(a + b)g}{I_s + (m_s + m_p)r^2} \tag{10}$$

At the end, by considering the moment of inertia of a thin spherical shell about its central axis $I_s = \frac{2}{3}m_s r^2$, (10) becomes:

$$\ddot{p}_s = \frac{\left(\frac{a}{r} + \frac{b}{r}\right)g}{1 + \frac{5}{3}\frac{m_s}{m_p}} \tag{11}$$

From Table 1, $\ddot{p} \geq 0.5$ m/s^2. Consider the Earth, where $g = 9.81$ m/s^2. By assuming $r = 0.25$ m, $a/r = 0.44$ and $b/r = 0.15$, from (11) one must have $m_s/m_p \leq 6.34$, which is easily verified for these types of mechanisms as m_p is usually greater than m_s. On Mars, it is $g = 3.72$ m/s^2, and the condition is $m_s/m_p \leq 2.03$, so even in this case the desired acceleration is possible. On the Moon, it is $g = 1.62$ m/s^2 and one has $m_s/m_p \leq 0.54$ is also realistic in practice. This result indicates that the minimum ratio (5) is also compatible with the requirement on the minimum acceleration.

Copyright ©2022 by Dr. Matteo Melchiorre. Published by the IAF, with permission and released to the IAF to publish in all forms.

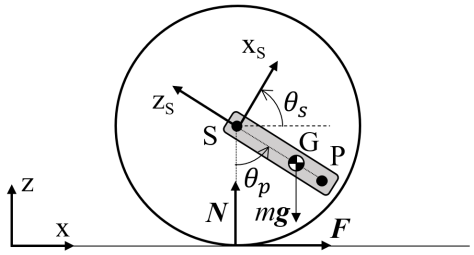

Fig. 4. Forces acting on the spherical robot actuated by single pendulum

4.2 Pendulum mechanism

The functional analysis has shown that a high value of a/r can be obtained with a light shell ($m_s \downarrow$) and a heavy pendulum ($m_p \uparrow$), possibly distributed close to the inner spherical surface ($b \uparrow$). This suggests placing actuators on the pendulum, far from the centre. In a classical configuration, as the one depicted in Fig. 5, this is not possible due to mechanical coupling between the motors and the gimbal.

In this work, a differential driving mechanism that allows to keep actuators on the pendulum is used. The mechanism is inspired by [8], but shows a more compact design and different power transmission components.

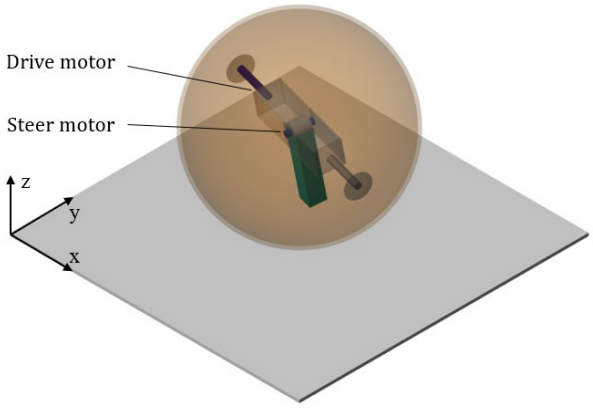

Fig. 5. Classical functional solution of the single pendulum mechanism

The differential driving mechanism is shown in Fig. 6a. The working principle is the same of the traditional one used on cars (see Fig. 6b), except that in the one applied to the spherical robot the carrier 4, i.e. the central shaft that supports the pendulum, is rigid with the planet gear 3. Moreover, in this case the sun gears 1 and 2 are the inputs and are supposed to be connected to two motors.

Let T_1, ω_1 , T_2, ω_2 and T_3, ω_3 denote torque and angular velocity of sun gears and planet gear about the direction of the drive axis. Let T_4, Ω indicate torque and angular velocity of the carrier about the steer axis. The following kinematic constraint holds:

$$\Omega = \frac{\omega_1 + \omega_2}{2} \tag{12}$$

Moreover, by observing Fig. a and Fig. , one can find:

$$\begin{cases} T_1 = r_d F_{31} \\ T_2 = r_d F_{32} \\ T_3 = r_d F_{13} - r_d F_{23} \\ T_4 = r_d F_{13} + r_d F_{23} \end{cases} \Rightarrow \begin{cases} T_1 = r_d F_{31} \\ T_2 = r_d F_{32} \\ T_3 = T_1 - T_2 \\ T_4 = T_1 + T_2 \end{cases} \tag{13}$$

where r_d is the pitch radius of miter gears. Conservation of energy gives:

$$T_1\omega_1 + T_2\omega_2 = T_3\omega_3 + T_4\Omega \tag{14}$$

By substituting (12) and (13) in (14), it is:

$$(T_1 - T_2)(\omega_1 - \omega_2 - 2\omega_3) = 0 \tag{15}$$

If $T_1 \neq T_2$, (15) is verified for:

$$\omega_3 = \frac{\omega_1 - \omega_2}{2} \tag{16}$$

Given ω_1 and ω_2, kinematic expressions (12) and (16) permit to find ω_3 and Ω. In particular, if $\omega_1 = -\omega_2$, i.e., gears 1 and 2 rotate with same magnitude but in opposite direction, it is $\Omega = 0$ and $\omega_3 = \omega_1 = -\omega_2$. This is the case where the central shaft of the sphere keeps horizontal. On the other hand, if $\omega_1 = \omega_2$ one has $\Omega = \omega_1 = \omega_2$ and $\omega_3 = 0$, i.e., the shaft rotates only around the steer axis. In practice, if $\omega_1 \neq \omega_2$ one has $\Omega \neq 0$ and $\omega_3 \neq 0$, thus the sphere rolls on curved paths.

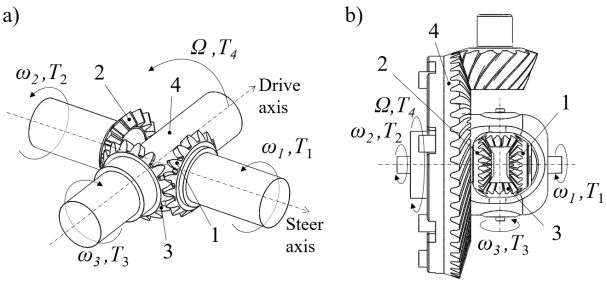

Fig. 6. Differential driving mechanism of the spherical robot (a). Traditional version used on cars (b)

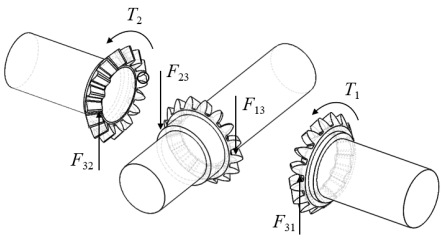

Fig. 7. Free body diagram of the differential driving mechanism of the spherical robot

Copyright ©2022 by Dr. Matteo Melchiorre. Published by the IAF, with permission and released to the IAF to publish in all forms.

5. Design of the spherical robot

This section describes the mechanical design and the mechatronic integration of the spherical robot. In the first part actuators, as well as structural and transmission components, are dimensioned. Successively, the design of the outer shell is shown. Finally, a schematic of the mechatronic integration with control units and batteries is proposed.

5.1 Mechanism design

The design solution of the differential gear together with power transmission and support components is shown in Fig. 8. Only one half of the chassis is shown. The mechanism has a total mass of 2 kg. In the following sections, some details on the design of the principal components are given.

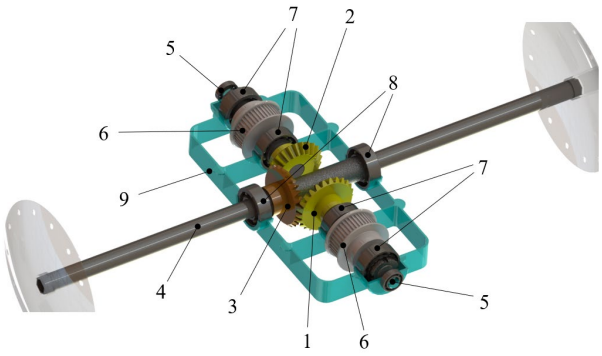

Fig. 8. Design solution of the differential gear. 1) - 2) Sun gears; 3) planet gear; 4) drive shaft; 5) steer shaft; 6) pulley; 7) steer shaft bearing; 8) drive shaft bearing; 9) chassis.

5.1.1 Actuators

The differential driving mechanism is thought to be actuated by two DC motors powering the sun gears. The size of the motors is designed in a worst-case condition, i.e., with $\varphi = 15°$ and $v_{max} = 2.5\ \mathrm{m/s}$. In this scenario, it is required a total torque T_3 equal to:

$$T_3 = rmg \sin\varphi \tag{17}$$

where resistive torque due to rolling friction has been neglected. From Table 1, by considering $m = 25$ kg and the Earth acceleration of gravity, the nominal power and the nominal torque required to each motor are:

$$P_n = \frac{mg \sin\varphi\, v_{max}}{2\eta_d \eta_t \eta_r} \simeq 95\ \mathrm{W} \tag{18}$$

$$T_n = \frac{P_n r}{\tau v_{max}} = \frac{9.5}{\tau}\ \mathrm{Nm} \tag{19}$$

where τ is the gear ratio, $\eta_d = 0.98$ is the efficiency of miter gears, $\eta_t = 0.95$ is one related to power transmission and $\eta_r = 0.9$ is the efficiency of the motor reducer.

When selecting the motor, it is good practice to consider a peak power twice as (18) to compensate for transient behaviours. The chosen motor is a DC brushed FAULHABER 3890 H024CR by Micromo, combined with a planetary gearhead with $\tau = 45$. The gear motor has a mass of $m_M = 0.88\ \mathrm{kg}$, an overall size $\phi 35 \times 166$ mm, a maximum continuous power of 160 W and a peak power of 381 W.

5.1.2 Differential gear

Miter gears have been designed according to ANSI/AGMA standards. Calculations have been made on the planet gear because it is the most stressed. The safety factor $s_G = 1.5$ has been used for bending and pitting resistance. The resulting gear is made of steel, has a module of 2 mm and 25 teeth, for a pitch diameter of 50 mm.

The drive shaft and the steer shafts, aligned to drive and steer axes respectively, have been dimensioned considering the stress produced in the maximum torque configuration and a pendulum mass $m_p = 20$ kg. The shafts are made of steel, have a diameter of 15 mm and a thickness of 2 mm.

The two motors are supposed to be placed on the pendulum, thus a power transmission to the steer shafts is needed. For the purpose, each motor is connected to miter gears by means of a timing belt and two pulleys. The selected timing belt is a GT3-3MGT with a length of 632 mm by Poggi. The pulley is selected from the same catalogue, it is made of aluminium and has a diameter of 42 mm.

5.2 Shell design

The shell must be sealed, light and able to deal with collisions. For this, a layer structure is adopted. The inner layer is made of sheets of harmonic steel, opportunely cutted in order to form a spherical frame when fixed to the lateral flanges (see Fig. 9a). The outer layer is provided with an impermeable rubber. The spherical shell has a total mass of 3.7 kg.

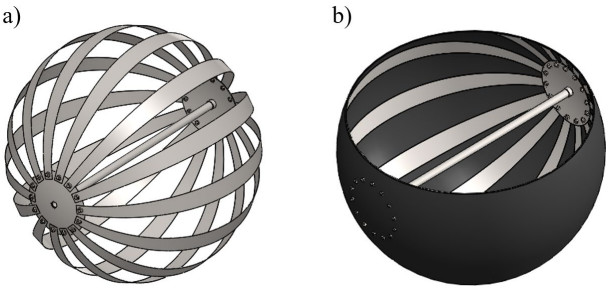

Fig. 9. Design of the spherical shell. a) Inner frame; b) section of the shell

Copyright ©2022 by Dr. Matteo Melchiorre. Published by the IAF, with permission and released to the IAF to publish in all forms.

5.3 Mechatronic integration

The electronic integration of the sensors has been presented in the dedicated chapter. In this section, energy storage and control units for the powering system is described.

The robot must be able to operate for 3 hours autonomously or remotely controlled. In the worst case, by observing (18), the total mechanical power provided by the two motors is 190 W, with an electrical efficiency of $\eta_e = 0.88$. By assuming that the robot operates with a mean power equal to half of the maximum power, the energy consumption is:

$$E = \frac{P_n}{\eta_e} \cdot 3\ \text{h} \simeq 324\ \text{Wh} \tag{20}$$

As the motors work at the tension of 24 V, in terms of electric charge:

$$E_{el} = \frac{E}{24\ \text{V}} = 13.5\ \text{Ah} \tag{21}$$

For the present case, a 16 Ah Li-Po rechargeable battery has been selected. The safety margin also takes into account a second controller and signal transmission devices for teleoperation. For instance, the first prototype will be tested on the Earth, so commercial devices have been considered. For wireless communication, the Xbee module can be used. An alternative solution with a radio remote controller receiver has also been considered. The mechatronics integration of power and control units is shown in Fig. 10. All the components can be placed on the pendulum. They have a total mass of 3.25 kg and sizes compatible with the internal volume of the sphere.

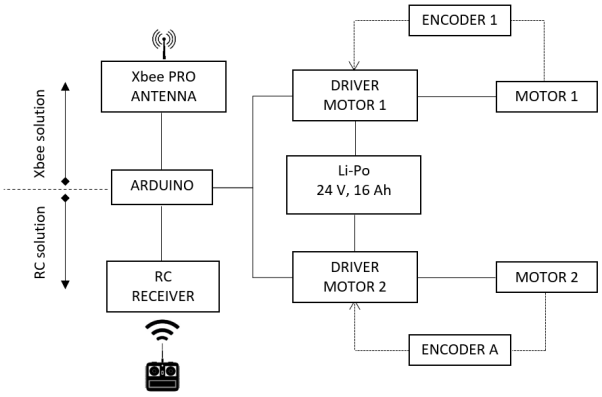

Fig. 10. Schematics of the mechatronics integration of power and control units

5.4 Design summary

The differential mechanism and the spherical shell form the mass $m_s = 5.7$ kg. The remaining mass for the pendulum is $m_p = 25\ \text{kg} - 5.7\ \text{kg} = 19.3\ \text{kg}$. With $r = 0.25$ m and $a/r = 0.44$, from (7) one calculates $b = 0.0325$ m. Therefore, the elements on the pendulum must be placed so that its centre of mass is at the minimum distance $a + b = 0.1425$ m from the sphere centre. The arrangement of the electronics will be addressed by future works. A possible configuration of the mechanical parts is shown in the assembly of Fig. 11 and Fig. 12.

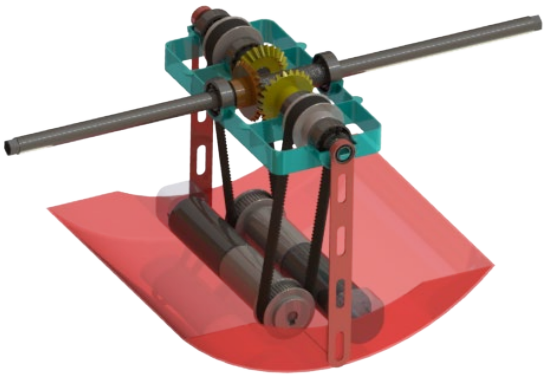

Fig. 11. Driving mechanism and pendulum

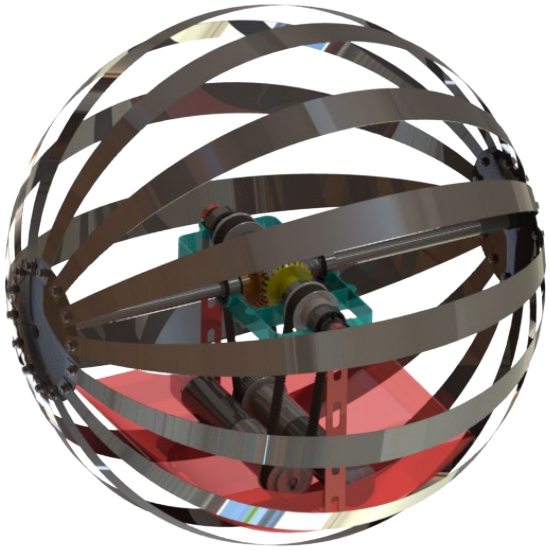

Fig. 12. Assembly of the spherical robot.

6. Results

A dynamic model of the robot has been implemented in Matlab-Simscape Multibody. The simulation environment is set so that the acceleration of gravity is the one on the Earth. Application on Moon and Mars will be addressed by future works, once the first outcomes from the real prototype will be available.

The mechanical parts of the robot in Fig. 12 have been imported in the model using *File Solid* blocks, that model a solid element starting from CAD files. The motors have been modelled according to the datasheet information.

Copyright ©2022 by Dr. Matteo Melchiorre. Published by the IAF, with permission and released to the IAF to publish in all forms.

The interaction between the robot and the terrain has been implemented using the *Sphere to Plane force* block of the contact force library [27]. It allows the bodies to exchange both normal forces and friction forces. Normal forces are modelled according to hertzian contact theory, while friction forces according to Stick-Slip phenomenon.

A feature of the model consists in the approach to step climbing. In Fig. 13 the schematization of a sphere of radius r climbing a step h is shown. The sphere is represented in three consecutive instants, drawn with different hatches. The center of the sphere S traces an arc having radius r.

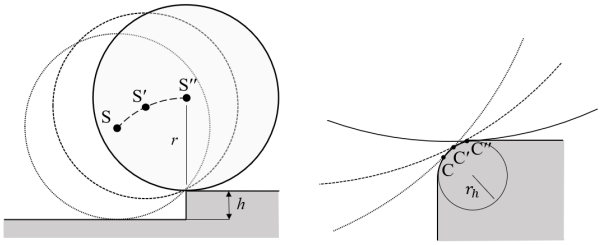

Fig. 13. Step climbing schematization

It is assumed that during the climb the step profile is a connection having radius r_h and the two bodies touch in points C, C′ and C″, performing actually a rolling motion. This phenomenon has been modelled in Matlab Simscape as the contact between a sphere and a cylinder, having radius r and r_h, respectively. The *Sphere to Tube Contact Force* block has been used.

The model can be used both as an instrument for supporting the design phase of the robot and for accurate simulations once the complete details of the project are defined. In the following, different tests results are proposed.

6.1 Rectilinear motion

The first test performed consists in performing a rectilinear path. According to equations (12) and (16), this occurs when the input velocities of the differential driving mechanism are equal and opposite. This corresponds to equal and opposite driving torques from the two motors. The test has been performed with data in Table 9. The mass of the sphere has been increased to $m_s = 6.5$ kg to compensate the weight of possible additional elements considered in a further design phase. The value of $(a + b)$ changes consequently.

In Fig. 14 and Fig. 15 results of the simulation are reported. In Fig. 14 the trajectory of the centre of mass of the robot is shown, while in Fig. 15 the oscillation of the pendulum centre of mass about the drive axis during the simulation is reported. As can be seen, it oscillates in the travel direction around an equilibrium position of about $\theta_{pd} = 2^{\circ}$, that is the value of the static equilibrium, in the case the sphere was still.

Table 9. Data for linear motion simulation

Parameter	Symbol	Value
Robot radius	r	0.25 m
Total mass	m	25 kg
Sphere mass	m_s	6.5 kg
Pendulum mass	m_p	18.5 kg
Inertia of the sphere	I_s	0.273 kgm^2
Position of the centre of mass of the robot	a	0.110 m
Position of the centre of mass of the pendulum	$a + b$	0.114 m
Driving torque motor 1	T_1	0.5 Nm
Driving torque motor 2	T_2	−0.5 Nm
Friction coefficient	μ	0.5
Simulation time	t_s	10 s

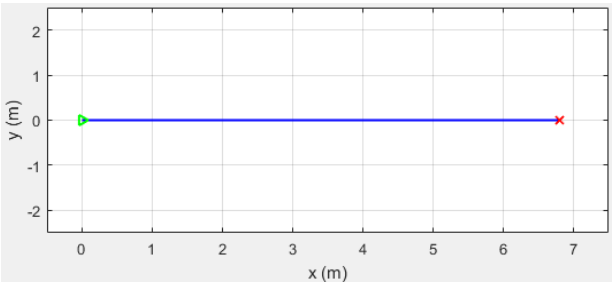

Fig. 14. Robot path of test with rectilinear motion

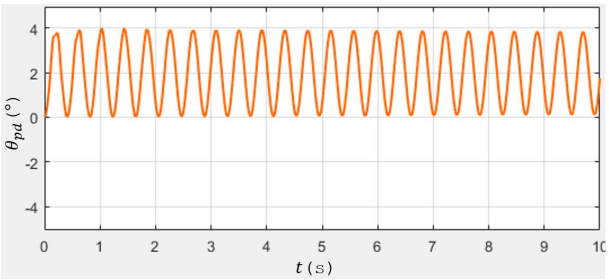

Fig. 15. Pendulum oscillation about the drive axis – rectilinear motion

6.2 Curved trajectory

In order to obtain a curved path, it is necessary to provide torque of different magnitude to the motors so that the pendulum rotates both around drive and steer axes. For instance, the test is carried out with the same values of Table 9, with the only difference that $T_2 = 0$ Nm.

In Fig. 16 four simulation frames are shown. In Fig. 17 the trajectory of the sphere center is reported, while in Fig. 18 the oscillation of the centre of mass of the pendulum about the steer axis θ_{ps} is shown (the one about the drive axis is not reported because close to zero). The central shaft tilts as the simulation starts and the robot turns almost in place by tracing a tight arc.

Copyright ©2022 by Dr. Matteo Melchiorre. Published by the IAF, with permission and released to the IAF to publish in all forms.

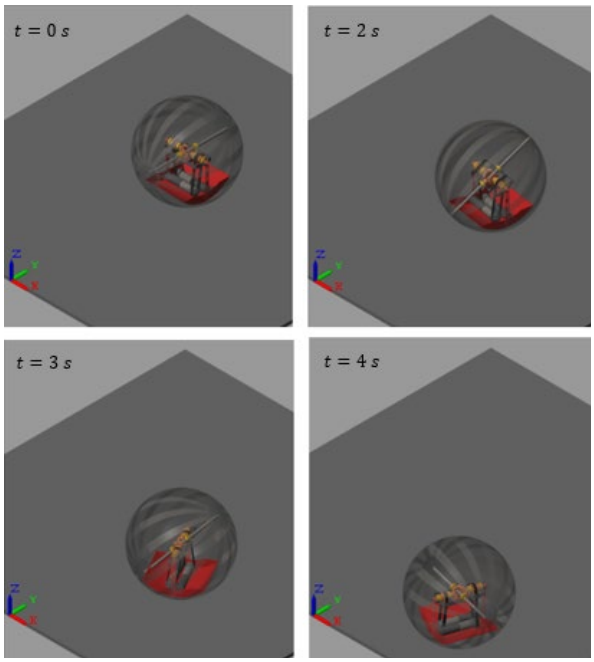

Fig. 16. Frames of the simulation of test with curved trajectory

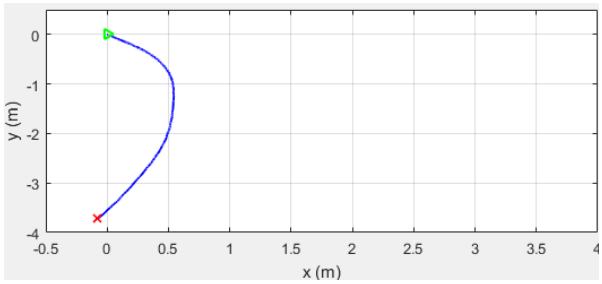

Fig. 17. Curved path of the robot

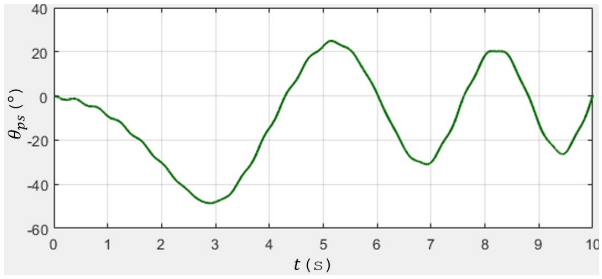

Fig. 18. Pendulum oscillation about the steer axis - test with curved trajectory

6.3 Step climbing

In this test the simulation starts with the robot in contact with the edge of the step and the pendulum in rest position. The step has a height h = 25 mm. In Fig. 19 some frames of the simulation are reported. A torque ramp is given to the motors as shown in Fig. 20. The robot can climb the step, and then moves on the horizontal plane.

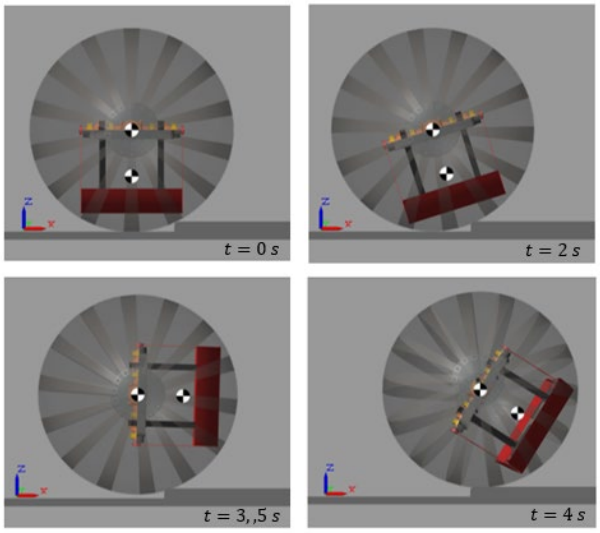

Fig. 19. Frames of the simulation – step climbing test

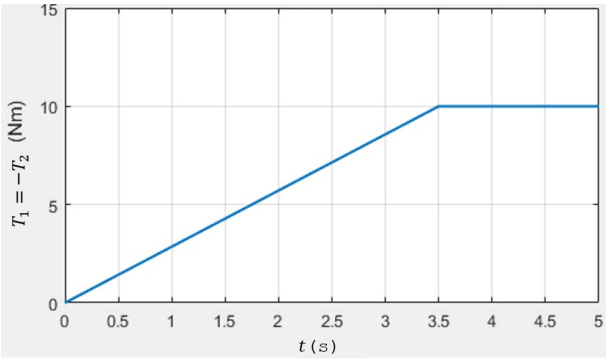

Fig. 20. Driving torques of the motors - step climbing test

7. Conclusions

The design of a pendulum-driven spherical robot has been presented. The advantages due to geometry make the robot particularly suitable for space exploration. For instance, the sphere hosts the mechanism, as well as dedicated sensors, in a sealed internal environment and is free from overturning. Moreover, it allows to deal with environmental objects such as stones or steps.

At the beginning, some mission specifications have been defined to outline robot weight, size and application. In particular, the robot must be able to climb inclined planes and steps and move on different types of terrain. From the study of the state of the art of spherical UGV, a trade-off analysis has been conducted and the driving mechanism for the robot has been selected. A single pendulum driven robot is the best solution for the application.

A functional analysis of the driving principle has shown that robot performances depend on geometry. In particular, the maximum torque is a function of the barycentre offset from the sphere center. To increase the offset, it is desirable to place actuators on the pendulum. Therefore, a differential mechanism has been used.

Copyright ©2022 by Dr. Matteo Melchiorre. Published by the IAF, with permission and released to the IAF to publish in all forms.

The mechanical design of the spherical robot has been described step by step. The mechatronic integration has involved electronic components for primarily tests to be made on the Earth.

A dynamic multibody model of the robot has been implemented in Matlab-Simscape to prove the validity of the mechanism and to show the robot operating in different conditions. Results collect different tests, such as linear motion, curved path and step climbing. The results confirms that the robot design meets the requirements on obstacles overcoming. Concerning steering capabilities, the robot is not omni-directional, but can turn almost in place thanks to the lateral swing of the pendulum and achieve a quasi omni-directionality.

Further works will primarily focus on the realization of the real prototype to be tested on the Earth. In the meantime, the analysis of robot performances in the martian and lunar environments can be carried out thanks to the simulation environment. Successively, electrical components of the robot will be reconsidered for spatial application.

References

[1] R. Chase and A. Pandya, "A review of active mechanical driving principles of spherical robots," *Robotics*, vol. 1, no. 1, pp. 3–23, 2012.

[2] J. Alves and J. Dias, "Design and control of a spherical mobile robot," in *Proceedings of the Institution of Mechanical Engineers. Part I: Journal of Systems and Control Engineering*, 2003, vol. 217, no. 6, pp. 457–467.

[3] X. Niu, A. P. Suherlan, G. S. Soh, S. Foong, K. Wood, and K. Otto, "Mechanical development and control of a miniature nonholonomic spherical rolling robot," in *2014 13th International Conference on Control Automation Robotics and Vision, ICARCV 2014*, 2014, pp. 1923–1928.

[4] A. Halme, T. Schonberg, and Y. Wang, "Motion control of a spherical mobile robot," in *Proceedings of 4th IEEE International Workshop on Advanced Motion Control - AMC '96 - MIE*, 1996, vol. 1, pp. 259–264.

[5] W. H. Chen, C. P. Chen, J. S. Tsai, J. Yang, and P. C. Lin, "Design and implementation of a ball-driven omnidirectional spherical robot," *Mech. Mach. Theory*, vol. 68, no. 1, pp. 35–48, 2013.

[6] Y. L. Karavaev and A. A. Kilin, "The dynamics and control of a spherical robot with an internal omniwheel platform," *Regul. Chaotic Dyn.*, vol. 20, no. 2, pp. 134–152, 2015.

[7] W. Liu, J. Sun, R. Wang, G. Geng, and X. Han, "Heavy-duty spherical mobile robot driven by five omni wheels," in *Proceedings of International Conference on Artificial Life and Robotics*, 2020, pp. 720–723.

[8] G. C. Schroll, "Design of a Spherical Vehicle with Flywheel Momentum Storage for High Torque Capabilities," Massachusetts Institute of Technology, 2008.

[9] V. Kaznov and M. Seeman, "Outdoor navigation with a spherical amphibious robot," *IEEE/RSJ 2010 Int. Conf. Intell. Robot. Syst. IROS 2010 - Conf. Proc.*, pp. 5113–5118, 2010.

[10] D. Pokhrel, N. R. Luitel, S. Das, and D. N. Ray, "Design and development of a spherical robot (SpheRobot)," *1st Int. 16th Natl. Conf. Mach. Mech. Ina. 2013*, pp. 735–741, 2013.

[11] A. P. Rossi *et al.*, "Daedalus - descent and exploration in deep autonomy of lava underground structures," 2021.

[12] B. Zhao, P. Wang, H. Hu, M. Li, and L. Sun, "Study on turning in place of a spherical robot based on stick-slip principle," in *2009 IEEE International Conference on Robotics and Biomimetics, ROBIO 2009*, 2009, pp. 771–775.

[13] S. Sang, J. Zhao, H. Wu, S. Chen, and Q. An, "Modeling and simulation of a spherical mobile robot," *Comput. Sci. Inf. Syst.*, vol. 7, no. 1, pp. 51–62, 2010.

[14] F. Tomik, S. Nudehi, L. L. Flynn, and R. Mukherjee, "Design, fabrication and control of spherobot: A spherical mobile robot," *J. Intell. Robot. Syst. Theory Appl.*, vol. 67, no. 2, pp. 117–131, 2012.

[15] M. Artusi, M. Potz, J. Aristiźabal, C. Menon, S. Cocuzza, and S. Debei, "Electroactive elastomeric actuators for the implementation of a deformable spherical rover," *IEEE/ASME Trans. Mechatronics*, vol. 16, no. 1, pp. 50–57, 2011.

[16] K. W. Wait, P. J. Jackson, and L. S. Smoot, "Self locomotion of a spherical rolling robot using a novel deformable pneumatic method," in *Proceedings - IEEE International Conference on Robotics and Automation*, 2010, pp. 3757–3762.

[17] K. Y. Ho and N. Michael Mayer, "Implementation of a mobile spherical robot with shape-changed inflatable structures," *Int. Conf. Adv. Robot. Intell. Syst. ARIS*, pp. 104–109, 2017.

[18] K. Halvorsen, "MorpHex MKIII," *Zenta Robotic Creations*, 2014. [Online]. Available: http://zentasrobots.com/robot-projects/morphex-mkiii. [Accessed: 24-Aug-2022].

[19] T. Aoki, S. Ito, and Y. Sei, "Development of quadruped walking robot with spherical shell-mechanical design for rotational locomotion," in *IEEE International Conference on Intelligent Robots and Systems*, 2015, pp. 5706–5711.

[20] N. Bun-Athuek and P. Laksanacharoen, "Simulation of a reconfigurable spherical robot

Copyright ©2022 by Dr. Matteo Melchiorre. Published by the IAF, with permission and released to the IAF to publish in all forms.

IV for confined environment," in *IEEE Region 10 Annual International Conference, Proceedings/TENCON*, 2020, pp. 1058–1062.

[21] M. Zhang, B. Chai, L. Cheng, Z. Sun, G. Yao, and L. Zhou, "Multi-movement spherical robot design and implementation," *Proc. 2018 IEEE Int. Conf. Mechatronics Autom. ICMA 2018*, pp. 1464–1468, 2018.

[22] C. J. Dudley, A. C. Woods, and K. K. Leang, "A micro spherical rolling and flying robot," in *IEEE International Conference on Intelligent Robots and Systems*, 2015, pp. 5863–5869.

[23] S. Sabet, M. Poursina, and P. E. Nikravesh, "Control of Spherical Robots on Uneven Terrains," in *IEEE International Conference on Intelligent Robots and Systems*, 2021, pp. 8159–8165.

[24] J. Antol *et al.*, "Low Cost Mars Surface Exploration: The Mars Tumbleweed," Hampton, Virginia, 2003.

[25] T. Li and W. Liu, "Design and Analysis of a Wind-Driven Spherical Robot with Multiple Shapes for Environment Exploration," *J. Aerosp. Eng.*, vol. 24, no. 1, pp. 135–139, 2011.

[26] T. Ylikorpi and J. Suomela, "Ball-shaped Robots," in *Climbing and Walking Robots: Towards New Applications*, H. Zhang, Ed. InTech, 2007, pp. 235–256.

[27] S. Miller, "Simscape Multibody Contact Forces Library." GitHub, 2022.